Nucleation of Chemically Active Droplets

Noah Ziethen, Jan Kirschbaum, and David Zwicker*
Max Planck Institute for Dynamics and Self-Organization, Am Faßberg 17 37077, Göttingen, Germany

(Received 23 December 2022; accepted 10 May 2023; published 16 June 2023)

Driven chemical reactions can control the macroscopic properties of droplets, like their size. Such active droplets are critical in structuring the interior of biological cells. Cells also need to control where and when droplets appear, so they need to control droplet nucleation. Our numerical simulations demonstrate that reactions generally suppress nucleation if they stabilize the homogeneous state. An equilibrium surrogate model reveals that reactions increase the effective energy barrier of nucleation, enabling quantitative predictions of the increased nucleation times. Moreover, the surrogate model allows us to construct a phase diagram, which summarizes how reactions affect the stability of the homogeneous phase and the droplet state. This simple picture provides accurate predictions of how driven reactions delay nucleation, which is relevant for understanding droplets in biological cells and chemical engineering.

DOI: 10.1103/PhysRevLett.130.248201

Droplets forming by phase separation are crucial to spatially structure the interior of biological cells, e.g., to separate molecules, control reactions, and exert forces [1–5]. Cells control phase separation using actively driven chemical reactions, which often include enzymes that modify biomolecules involved in phase separation [6–8]. Theoretical work showed that such reactions can control droplet sizes and their general macroscopic behavior [9–15]. In contrast, how these droplets emerge is little understood. Experiments suggest that droplets form by nucleation [16], but to what extent reactions can regulate nucleation is unclear.

Nucleation is a stochastic process that relies on thermal fluctuations to create a sufficiently large nucleus that can grow spontaneously [17–19]. This is because creating the droplet interface costs energy, so tiny droplets generally dissolve. Classical nucleation theory predicts that the typical nucleation time scales exponentially with the energy barrier associated with the critical nucleus. While this theory is well understood for passive systems, it is unclear how it can be extended to active systems, where free energies are generally unavailable. To overcome this challenge, we use an equilibrium surrogate model to reveal how driven reactions controlling droplet size suppress nucleation substantially.

We study an isothermal fluid comprised of precursor material A that can convert into droplet material B by chemical reactions. For simplicity, we first consider an incompressible fluid where both species have equal molecular volume ν, so the state of the system is characterized by the concentration $c(\boldsymbol{r}, t)$ of species B, while the concentration of A is $\nu^{-1} - c(\boldsymbol{r}, t)$. The dynamics are governed by the continuity equation

$$\partial_t c + \nabla \cdot \boldsymbol{j} = s, \tag{1}$$

where $\boldsymbol{j}$ denotes the diffusive exchange flux and the source term s describes chemical transitions.

The passive diffusive flux $\boldsymbol{j}$ is driven by the gradient of the chemical potential, $\boldsymbol{j} = -\Lambda_\mathrm{d} \nabla \mu + \boldsymbol{\eta}$, where Λ_d is the diffusive mobility and $\boldsymbol{\eta}$ is the diffusive thermal noise, which obeys $\langle \eta_i(\boldsymbol{r}, t) \rangle = 0$ and the fluctuation dissipation theorem $\langle \eta_i(\boldsymbol{r}, t) \eta_j(\boldsymbol{r}', t') \rangle = 2 k_\mathrm{B} T \Lambda_\mathrm{d} \delta_{ij} \delta(\boldsymbol{r} - \boldsymbol{r}') \delta(t - t')$ [20–22].

The exchange chemical potential, $\mu = \delta F[c]/\delta c$, follows from the free energy functional [13]

$$F[c] = \int \left[f(c) + \frac{\kappa}{2} |\nabla c|^2 \right] \mathrm{d}\boldsymbol{r}, \tag{2}$$

where $f(c)$ is the local free energy density and κ penalizes compositional gradients. For simplicity, we consider

$$f(c) = a_1 c - \frac{a_2}{2} \left(c - \frac{1}{2\nu} \right)^2 + \frac{a_4}{4} \left(c - \frac{1}{2\nu} \right)^4, \tag{3}$$

where a_1, a_2, and $a_4 > 0$ are phenomenological coefficients. Without reactions ($s = 0$), Eqs. (1)–(3) describe passive phase separation with a critical point at $c_\mathrm{crit} = (1/2\nu)$ for $a_2 = 0$. For $a_2 > 0$, the spinodal line is given by $c_\mathrm{sp} = (1/2\nu) \pm \sqrt{a_2/(3a_4)}$, and the binodal is defined by coexisting equilibrium concentrations $c_\mathrm{out} = (1/2\nu) - \sqrt{a_2/a_4}$ and $c_\mathrm{in} = (1/2\nu) + \sqrt{a_2/a_4}$ in dilute and dense

phases, respectively. These phases are separated by an interface of width $w = \sqrt{2\kappa/a_2}$.

The system becomes active when phase separation is augmented by driven chemical reactions. As an example, we first consider a reaction flux s comprising passive conversion of A and B as well as an active conversion involving chemical energy $\Delta\mu$ provided by a fuel [14],

$$s(c) = -\Lambda_r^p \mu - \Lambda_r^a c\,(\mu + \Delta\mu) + \eta_r(c), \tag{4}$$

where Λ_r^p and Λ_r^a determine the rates of the respective reactions and η_r models thermal fluctuations. Motivated by enzymes that colocalize with the droplet, we scale the rate of the active reaction with the concentration c of the droplet material. This results in a minimal, thermodynamically consistent model where droplet material B turns into precursor A inside droplets, while B is replenished outside, thus controlling droplet size [14]. The reactive thermal noise η_r obeys $\langle \eta_r(\boldsymbol{r}, t)\rangle = 0$ and $\langle \eta_r(\boldsymbol{r}, t)\eta_r(\boldsymbol{r}', t')\rangle = 2k_B T\Lambda_r \delta(\boldsymbol{r} - \boldsymbol{r}')\delta(t - t')$ with $\Lambda_r(c) = \Lambda_r^p + \Lambda_r^a c$. We here consider the typical situation of size-controlled droplets, where diffusion dominates reactions [14]. In particular, diffusive noise dominates below the length scale $(\Lambda_d/\Lambda_r)^{1/2}$, which is larger than $10w$ for the parameters discussed here. Since critical nuclei are much smaller, we neglect reactive noise in the following, approximating reactions as deterministic. Figure 1(a) shows that the reaction flux s given in Eq. (4) is a nonmonotonous function of the composition c. In particular, there are two stable homogeneous stationary states, which correspond to (meta-)stable dilute and dense systems. The main question in this Letter concerns how active droplets nucleate from the dilute homogeneous state $c(\boldsymbol{r}) = c_0$.

To investigate nucleation, we first perform numerical simulations of Eqs. (1)–(4) in a two-dimensional system with periodic boundary conditions [23]; see Fig. 1(b). Repeating the simulations many times, we observe that the first droplet nucleates at random times t_{nucl}; see Fig. 1(c). Assuming an exponential distribution of t_{nucl}, we define the nucleation time τ as the ensemble average of t_{nucl}. Figure 1(d) shows that τ increases for stronger interactions (larger a_2), as expected for nucleation of passive droplets [24]. More importantly, larger reaction rates lead to longer nucleation times τ, indicating that active chemical reactions hinder nucleation. This result can be understood intuitively since the reactions stabilize the homogeneous state; see Fig. 1(a). They thus help to dissolve a small accumulation of droplet material B, reducing the probability that a critical nucleus forms.

To quantitatively predict the effect of driven reactions on nucleation, we next map our system to an approximate equilibrium system. To do this, we linearize the reaction flux s around the dilute homogeneous stationary state c_0,

$$s_{\mathrm{lin}}(c) = k(c_0 - c) \quad \text{with} \quad k = -s'(c_0), \tag{5}$$

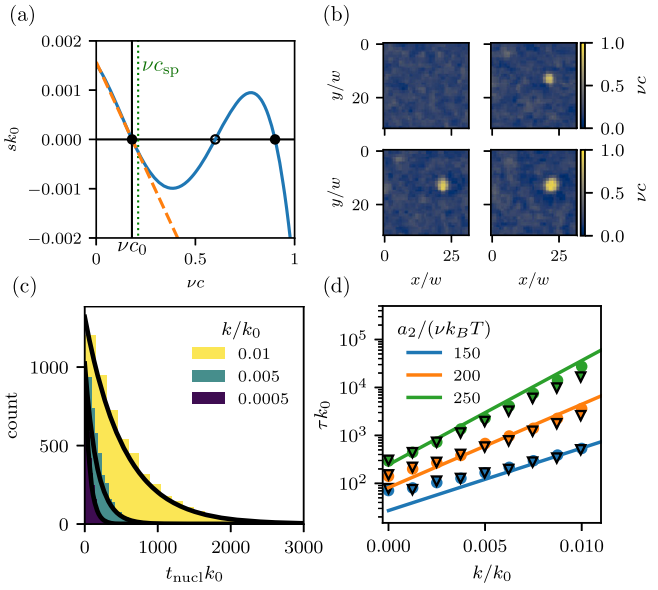

FIG. 1. Chemical reactions increase nucleation times. (a) Reaction flux s as a function of the concentration c of a homogeneous system for the full [solid blue line, Eq. (4)] and linearized model (dashed orange line). The spinodal concentration c_{sp} of the passive system (dotted green line), the two stable fixed points (filled disks), and the unstable fixed point (open circle) are marked. (b) Snapshots of the concentration field c of droplet material obtained from stochastic numerical simulation in two dimensions. The time between snapshots is $10/k_0$, and the interaction strength is $a_2 = 200\nu k_B T$. (c) Distribution of measured nucleation times t_{nucl} in the linearized model for various reaction rates k for $a_2 = 150\nu k_B T$. Black lines show exponential distributions of equivalent mean $\tau = \langle t_{\mathrm{nucl}}\rangle$. (d) Nucleation time τ as a function of k for the full model [disks, $k = -s'(c_0) \propto \Lambda_r^a$] and the linearized reactions (triangles) for various interaction strengths $a_2/(\nu k_B T)$. Solid lines show predictions of Eq. (7) with τ_0 as a single fit parameter for all curves. (a)–(d) Additional parameters are $a_1\nu = -1.34a_2$, $a_4 = 4a_2\nu$, $\Lambda_r^p/\Lambda_r^a = 0.0311$, $\Delta\mu\nu = 1.46a_2$, $\nu = w^2$, $w = \sqrt{2\kappa/a_2}$, and $k_0 = \Lambda_d a_2 w^{-2}$.

where $k > 0$ for a stable state; see Fig. 1(a). Figure 1(d) shows that the linearized reactions influence the nucleation time τ similarly to the full reaction flux s. The linearization allows us to map the dynamics given by Eq. (1) to a passive system, $\partial_t c \approx \Lambda_d \nabla^2 \delta\tilde{F}[c]/\delta c$, with the augmented free energy functional

$$\tilde{F}[c] = F[c] + \frac{k}{2\Lambda_d}\int [c(\boldsymbol{r}) - c_0]\Psi(\boldsymbol{r})\mathrm{d}\boldsymbol{r}, \tag{6}$$

where Ψ obeys the Poisson equation $\nabla^2\Psi = c_0 - c(\boldsymbol{r})$ and thus mediates long-ranged, Coulomb-like interactions [25–27].

We use the equilibrium surrogate model to investigate the energy landscape of nucleation. In particular, we use Eq. (6) to map the minimal energy path connecting the metastable homogeneous state with the equilibrium state

containing one droplet using a proxy for droplet size as a reaction coordinate x [28]. For each value of x, we use a constrained optimization to determine the spherically symmetric composition $c(r)$ that minimizes the energy $\tilde{F}$ given by Eq. (6). Figure 2(a) shows that the resulting profiles feature an increasing density peak, analogous to passive systems [19]. However, the nucleus is also surrounded by a depletion zone originating from chemical reactions. The sequence of profiles defines the minimal energy path, from which we obtain the energy barrier ΔF as the difference between the maximal energy and the energy $\tilde{F}(x=0)$ of the homogeneous state; see Fig. 2(b). Figure 2(c) shows that the energy barrier ΔF depends on the reaction rate k, and this dependence is approximately linear [Fig. 2(d)], suggesting that the long-ranged term in Eq. (6) could explain the suppressed nucleation caused by reactions.

We hypothesize that the increasing energy barriers explain how larger reaction rates k lead to longer nucleation times τ [see Fig. 1(d)]. Nucleation theory predicts that τ increases exponentially with the energy barrier ΔF [24],

$$\tau = \tau_0 \exp\left(\frac{\Delta F}{k_B T}\right), \tag{7}$$

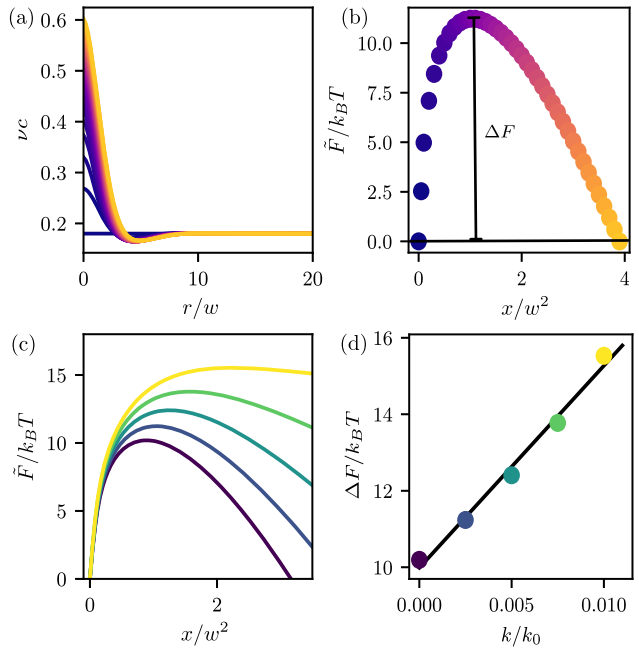

FIG. 2. Reactions increase free energy barrier ΔF of surrogate equilibrium model. (a) Radial concentration profiles $c(r)$ minimizing the free energy $\tilde{F}$ given by Eq. (6) at various fixed values of reaction coordinate x [colors correspond to panel (b)]. (b) $\tilde{F}$ as a function of x with ΔF indicated. (c) $\tilde{F}(x)$ for various reaction rates k [colors correspond to panel (d)]. (d) ΔF as a function of k. (a)–(d) Model parameters are $c\nu = 0.18$, $L = 100w$, $a_2 = 250\nu k_B T$, $k = 0.0025 k_0$ [for panels (a) and (b)] and are given in Fig. 1.

where τ_0 is a kinetic prefactor. Figure 1(d) shows that this relation explains the numerical data, particularly for larger ΔF at higher k and a_2. The deviation at smaller k are expected since the assumptions leading to Eq. (7) break down for smaller ΔF [19]. We conclude that the energy barriers derived from the equilibrium surrogate model explain how nucleation times increase with reaction rates.

Motivated by the success of nucleation theory, we next seek an analytical description of the free energy barrier, using the radius R of a droplet as a reaction coordinate. Assuming that the droplet with homogeneous concentration c_{in} is embedded in an infinite system of concentration c_0, the free energy $\tilde{F}$ can be separated into contributions of bulk phases, interface, and chemical reactions,

$$\tilde{F}(R) \approx -gV + \gamma A + F_{\text{react}}(R), \tag{8}$$

where $V = \pi R^2$ and $A = 2\pi R$ in two dimensions [28]. Classical nucleation theory implies the free energy difference $g = f(c_0) - f(c_{\text{in}}) + \mu(c_0)(c_{\text{in}} - c_0)$ between the phases and surface tension $\gamma = \sqrt{8\kappa a_2^3}/(3a_4)$ [13], which is a good approximation for $c_0 \approx c_{\text{out}}$. We derive an approximate expression for the free energy associated to reactions in the Supplemental Material [28],

$$F_{\text{react}}(R) \approx \frac{\pi(c_{\text{in}} - c_0)^2}{16\Lambda_d} k R^4, \tag{9}$$

where we neglected terms proportional to $k(c_{\text{out}} - c_0)^2$. Without reactions ($k = 0$), $\tilde{F}(R)$ given by Eq. (8) has a single maximum at the critical radius $R_{\text{crit}}^{\text{pas}} = \gamma/g$ with a corresponding energy barrier $\Delta F = \pi\gamma^2/g$; see Fig. 3(a). Once nuclei exceed this critical size (by nucleation), they grow indefinitely. In contrast, Eq. (8) predicts that reactions ($k > 0$) increase the free energy of large droplets, implying a minimum at finite radius $R_{\text{stab}} \approx (c_0 - c_{\text{in}})^{-2}[8g\Lambda_d/k]^{1/2}$ corresponding to stable droplets [10]. Concomitantly, the energy barrier ΔF is elevated, consistent with increased nucleation times. Approximating the barrier by $\tilde{F}(R_{\text{crit}}^{\text{pas}})$, we find

$$\Delta F \approx \frac{\pi\gamma^2}{g}\left[1 + k\frac{\gamma^2(c_{\text{in}} - c_0)^2}{16 g^3 \Lambda_d}\right], \tag{10}$$

which explains the linear dependence of ΔF on k observed in Fig. 2(d). Taken together, this simplified picture demonstrates how large rates k gradually disfavor the droplet state until only the homogeneous state remains stable at $k > k_{\max}$ with $k_{\max} = 32\Lambda_d g^3/[27\gamma^2(c_{\text{in}} - c_0)^2]$.

Finally, we use the simplified free energy of the equilibrium surrogate model to study the influence of the concentration c_0 of the homogeneous state. In particular, we determine the minimal value of c_0 beyond which the droplet state can be stable as a function of the interaction

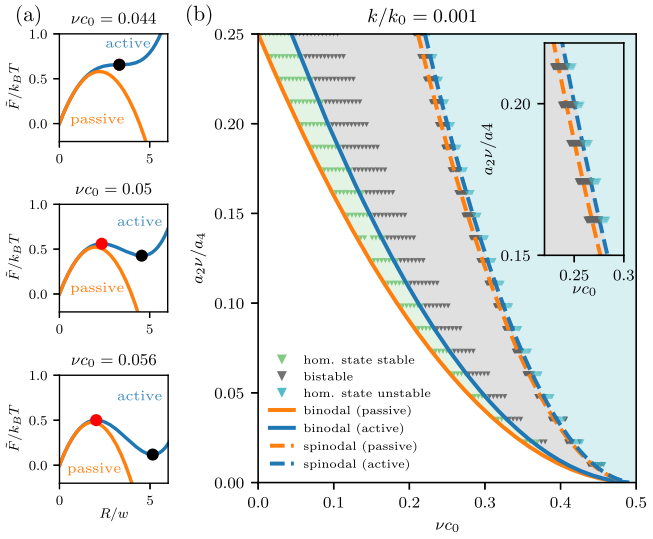

FIG. 3. Extended phase diagram accounting for reactions. (a) Free energy $\tilde{F}$ of the surrogate equilibrium model approximated by Eq. (8) as a function of the nucleus radius R for decreasing concentrations c_0 of the homogeneous state (bottom to top) and $a_2\nu/a_4 = 0.25$. (b) Extended phase diagram indicating the stability of the homogeneous and droplet state as a function of c_0 and $a_2\nu/a_4$ in a passive (orange lines, $k = 0$) and active system (blue lines, $k = 10^{-3}k_0$). The droplet state is (meta-)stable right of the solid (binodal) lines, while the homogeneous state is stable left of the dashed (spinodal) lines. Behavior of numerical simulations (symbols) for $k = 10^{-3}k_0$ corroborate the results. Inset shows enlarged region around the spinodal. (a)–(b) Additional model parameters are given in Fig. 1.

parameter a_2. In passive systems ($k = 0$), the resulting line corresponds to the binodal curve. In active systems ($k > 0$), this line is shifted to larger concentrations, thus enlarging the region where the homogeneous state is stable. The homogeneous state becomes unstable at the spinodal line, which can be determined from a linear stability analysis of Eq. (1) [28]. Figure 3(b) shows that these predictions based on Eq. (8) agree with numerical simulations probing the stability of the homogeneous and droplet state. Both predictions illustrate how driven chemical reactions destabilize the droplet state.

In summary, we illuminated how driven chemical reactions affect the phase diagram of phase separating systems. To do this, we exploited the equilibrium surrogate of the active system to show how reactions favor the homogeneous state relative to the droplet state, which explains the suppressed nucleation qualitatively. Similar behavior was found for an equilibrium system with true long-ranged interactions [27]. Although the modified phase diagram was derived from the surrogate model, it is not a thermodynamic phase diagram of the phase separating system with driven reactions. For instance, the compositions of the coexisting phases at the interface are still governed by the binodal and tie lines of the passive phase diagram [13]. The energy barrier associated with reactions depends linearly on their rate k, likely because reactions are weak and the system is dominated by phase separation. This implies that k decreases nucleation rates exponentially. We showed that this dependence persists for thermodynamically consistent reactions and expect that it is a general feature of phase separating systems with reactions that have a stable dilute phase. As a proof of concept, we show in the Supplemental Material [28] that a three-component system exhibits very similar suppression of nucleation. Since our derivation of the influence of the reactions is independent of the details of the free energy density, we expect equivalent behavior in a wide range of phase separating systems.

We presented results for the simple case of two-dimensional systems. While we expect that active reactions also suppress nucleation in more complicated situations, it will be vital to extend our theory to three dimensions (e.g., to capture spontaneous divisions [11]) and many components (allowing for additional stable stationary states [14,15]). For better quantitative agreement, it might also be necessary to improve our treatment of nucleation theory, e.g., by describing how reactions affect the curvature of the surrogate free energy, which affects nucleation rates via the Zeldovich factor [31]. However, the ultimate test of our theory will come from experiments, either from existing active droplets in biological cells [32] or in promising synthetic systems [33,34]. Experiments in cells also suggest that more complex behaviors are possible, including periodic nucleation [35] and multistep nucleation for fiber formation [36], which might involve secondary nucleation [37]. In these situations, heterogeneous nucleation is likely relevant [38,39], and there are examples where nucleation is controlled by catalytically active nucleation sites [9,40]. Taken together, our approach of an equilibrium surrogate model will likely prove vital for studying nucleation in these more challenging situations.

The chemically active droplets we discuss here are exemplary for nonequilibrium phase separation. Our model is similar to a recent study that finds that reactions accelerate nucleation [41]. However, they consider fixed supersaturation instead of fixed average composition, and their grand canonical scheme might not capture the reaction-diffusion dynamics accurately. Both models combine conservative phase separation with nonconservative reactions, and are thus related to the generic Active Model AB [42]. In the limit of fast reactions, these models are predicted to be related to the conservative Active Model B+ [43], whose nucleation has recently been studied [44], but it is unlikely that this analogy holds for the relevant case of weak reactions. Taken together, these works provide intriguing avenues for future work studying the differences and similarities of active phase separating systems.

We thank Kristian Blom, Aljaz Godec, and Micheal Cates for helpful discussions and Gerrit Wellecke for a critical reading of the manuscript. We gratefully

acknowledge funding from the Max Planck Society, the European Union (ERC, EmulSim, 101044662), and the German Research Foundation (DFG) under Grant Agreement No. ZW 222/3.

*david.zwicker@ds.mpg.de

[1] C. P. Brangwynne, C. R. Eckmann, D. S. Courson, A. Rybarska, C. Hoege, J. Gharakhani, F. Julicher, and A. A. Hyman, Science **324**, 1729 (2009).
[2] A. A. Hyman, C. A. Weber, and F. Jülicher, Annu. Rev. Cell Dev. Biol. **30**, 39 (2014).
[3] S. F. Banani, H. O. Lee, A. A. Hyman, and M. K. Rosen, Nat. Rev. Mol. Cell Biol. **18**, 285 (2017).
[4] G. L. Dignon, R. B. Best, and J. Mittal, Annu. Rev. Phys. Chem. **71**, 53 (2020).
[5] Q. Su, S. Mehta, and J. Zhang, Mol. Cell **81**, 4137 (2021).
[6] M. Hondele, R. Sachdev, S. Heinrich, J. Wang, P. Vallotton, B. M. A. Fontoura, and K. Weis, Nature (London) **573**, 144 (2019).
[7] W. T. Snead and A. S. Gladfelter, Mol. Cell **76**, P295 (2019).
[8] J. Söding, D. Zwicker, S. Sohrabi-Jahromi, M. Boehning, and J. Kirschbaum, Trends Cell Biol. **30**, S0962892419301795 (2019).
[9] D. Zwicker, M. Decker, S. Jaensch, A. A. Hyman, and F. Jülicher, Proc. Natl. Acad. Sci. U.S.A. **111**, E2636 (2014).
[10] D. Zwicker, A. A. Hyman, and F. Jülicher, Phys. Rev. E **92**, 012317 (2015).
[11] D. Zwicker, R. Seyboldt, C. A. Weber, A. A. Hyman, and F. Jülicher, Nat. Phys. **13**, 408 (2017).
[12] J. D. Wurtz and C. F. Lee, Phys. Rev. Lett. **120**, 078102 (2018).
[13] C. A. Weber, D. Zwicker, F. Jülicher, and C. F. Lee, Rep. Prog. Phys. **82**, 064601 (2019).
[14] J. Kirschbaum and D. Zwicker, J. R. Soc. Interface **18**, 20210255 (2021).
[15] D. Zwicker, Curr. Opin. Colloid Interface Sci. **61**, 101606 (2022).
[16] S. F. Shimobayashi, P. Ronceray, D. W. Sanders, M. P. Haataja, and C. P. Brangwynne, Nature (London) **599**, 503 (2021).
[17] R. P. Sear, J. Phys. Condens. Matter **19**, 033101 (2007).
[18] X. Xu, C. L. Ting, I. Kusaka, and Z.-G. Wang, Annu. Rev. Phys. Chem. **65**, 449 (2014).
[19] V. Kalikmanov, Lect. Notes Phys. **860**, 1 (2013).
[20] F. Jülicher, S. W. Grill, and G. Salbreux, Rep. Prog. Phys. **81**, 076601 (2018).
[21] S. R. De Groot and P. Mazur, *Non-Equilibrium Thermodynamics* (Dover Publications, New York, 1984).
[22] *Solids Far from Equilibium*, Collection Aléa-Saclay (Cambridge University Press, Cambridge, New York, 1991).
[23] D. Zwicker, J. Open Source Software **5**, 2158 (2020).
[24] S. Arrhenius, Z. Phys. Chem. **4U**, 226 (1889).
[25] F. Liu and N. Goldenfeld, Phys. Rev. A **39**, 4805 (1989).
[26] J. J. Christensen, K. Elder, and H. C. Fogedby, Phys. Rev. E **54**, R2212 (1996).
[27] C. B. Muratov, Phys. Rev. E **66**, 066108 (2002).
[28] See Supplemental Material at http://link.aps.org/supplemental/10.1103/PhysRevLett.130.248201 for details on the constrained optimization, derivation of Eq. (9), classical nucleation theory extended by chemical reactions, linear stability analysis with reactions, and suppressed nucleation in a three-component system, which includes Refs. [15,23,29,30].
[29] E. Vidal-Henriquez and D. Zwicker, Proc. Natl. Acad. Sci. U.S.A. **118**, e2102014118 (2021).
[30] S. Mao, D. Kuldinow, M. Haataja, and A. Košmrlj, Soft Matter **15**, 1297 (2018).
[31] J. Zeldovich, Sov. Phys. JETP **12**, 525 (1942).
[32] J. D. Wurtz and C. F. Lee, New J. Phys. **20**, 045008 (2018).
[33] C. Donau and J. Boekhoven, Trends Chem. **5**, P45 (2022).
[34] K. K. Nakashima, M. H. I. van Haren, A. A. M. André, I. Robu, and E. Spruijt, Nat. Commun. **12**, 3819 (2021).
[35] V. T. Yan, A. Narayanan, T. Wiegand, F. Jülicher, and S. W. Grill, Nature (London) **609**, 597 (2022).
[36] E. W. Martin, T. S. Harmon, J. B. Hopkins, S. Chakravarthy, J. J. Incicco, P. Schuck, A. Soranno, and T. Mittag, Nat. Commun. **12**, 4513 (2021).
[37] C. Weber, T. Michaels, and L. Mahadevan, eLife **8**, e42315 (2019).
[38] Y. Qi and B. Zhang, Nat. Commun. **12**, 6824 (2021).
[39] M.-T. Wei, Y.-C. Chang, S. F. Shimobayashi, Y. Shin, A. R. Strom, and C. P. Brangwynne, Nat. Cell Biol. **22**, 1187 (2020).
[40] D. Zwicker, J. Baumgart, S. Redemann, T. Müller-Reichert, A. A. Hyman, and F. Jülicher, Phys. Rev. Lett. **121**, 158102 (2018).
[41] Y. Cho and W. M. Jacobs, Phys. Rev. Lett. **130**, 128203 (2023).
[42] Y. I. Li and M. E. Cates, J. Stat. Mech. (2020) 053206.
[43] H. Alston, A. O. Parry, R. Voituriez, and T. Bertrand, Phys. Rev. E **106**, 034603 (2022).
[44] M. E. Cates and C. Nardini, Phys. Rev. Lett. **130**, 098203 (2023).